Design of Experiments for Supersonic ORC Nozzles in Linear Cascade Configuration

Marco Manfredi, Giacomo Persico, Andrea Spinelli*, Paolo Gaetani, Vincenzo Dossena

Politecnico di Milano, Energy Department, 20156, Milano, Italy

* Corresponding Author: andrea.spinelli@polimi.it

ABSTRACT

Small-scale Organic Rankine cycles (ORCs) are recognized as a promising solution to recover thermal energy from internal combustion engines (ICEs) in the transportation field, especially on-board of innovative long-haul trucks. Design methods for ORCs typically aim at obtaining good performance at both design and off-design operating conditions, especially in the frequent case of variable heat source flow rate and temperature. The fluid dynamic design of ORC turbines, whose performance considerably impacts on cycle efficiency, is usually performed by exploiting meanline models to define a baseline geometry, followed by the application of CFD-based shape optimization techniques. However, the validation of both low and high-fidelity tools is limited, due to a lack of experimental data. To fill this gap, an experimental campaign on supersonic ORC nozzle cascade was started at Politecnico di Milano. This paper comprehensively describes the methodologies applied to set-up an innovative linear cascade experiment, representative of the stator operation of axial/radial turbo-expanders for ORC systems. The selected working fluid is siloxane MM. Due to the nature of the flow, which feature complex shock patterns, and to the intrinsic challenge of performing measurements in close-to-critical point regions, several issues need to be solved to properly set-up the experiments. Cascade operating conditions to be investigated during the experiments are reported, as well as the methodology to set-up the test section, namely blade number, stagger angle, blade and side wall profiles. Main objective of experiments is to retrieve nozzle total pressure losses, in order to have a first validation of numerical simulations in terms of entropy production. A relatively high space resolution for measuring points is obtained downstream the cascade. Measurement technique selected include supersonic total pressure probes and wall pressure taps, as well as thermocouples and schlieren visualization. This paper reviews all steps required to design the campaign and aims at serving as a reference for future experimental investigations on ORC cascades. Main result of this preliminary work is the implementation of a relatively simple methodology to carry out experiments in blade cascade operated with organic vapors and aimed at evaluating row losses, without resorting to specifically calibrated instrumentation.

1. INTRODUCTION

As it is well known, the expander represents a crucial component in organic Rankine cycle (ORC) power systems and its efficiency strongly impacts on overall cycle performance and plant profitability (Colonna et al., 2015; Macchi and Astolfi, 2017). Utmost attention is therefore usually payed to its fluid dynamic design and high-fidelity design/optimization tools based on computational fluid dynamics (CFD) are nowadays largely employed. However, during preliminary system design, which involve fluid selection, cycle layout definition, specification of component architecture (heat exchanger, fluid machines) and their initial sizing, the high computational effort typical of high-fidelity expander design tools prevent their integration in the overall optimization process, due to the considerable number of simulations initially required. A viable option to integrate the expander preliminary optimization within the ORC

system design consists in the adoption of reduced-order methods, capable of providing machine preliminary geometry, efficiency, and off-design performance with a reduced computational cost. Referring to turbo-expanders, preferred for high temperature/high expansion ratio ORCs and under study in the presented research, such tools are the so called mean-line methods (Glassman, 1995; Ventura et al., 2012; Meroni et al., 2018). These models and their results can be easily integrated, possibly in the form of look-up tables, within cycle optimization loops (La Seta et al., 2016; White and Sayma, 2019). The capability and reliability of reduced-order models in correctly predicting turbine efficiency depend on the effectiveness and ranges of validity of the adopted loss correlations. Several loss models, spanning a wide range of empiricism level, are available in literature for both axial and radial turbine architectures (Ainley and Mathieson, 1951; Vavra, 1969; Craig and Cox, 1970; Glassman, 1976; Baines et al., 1998). The weakness of such relations is that they were developed for machines operating with conventional fluids and validated against test cases concerning standard gas or steam turbines, while their verification against experimental data over ORC expanders is largely lacking. An approach commonly adopted is to validate reduced-order models and loss correlations using high-fidelity CFD simulations (Fiaschi et al., 2012; De Servi et al., 2019). However, the verification of CFD simulations relies only on the accuracy of state-of-the-art thermodynamic fluid models (Span and Wagner, 2003) or, at most, on experimental data related to paradigmatic compressible flows, such as isentropic nozzle expansions (Spinelli et al., 2018; Robertson et al., 2019; Beltrame et al., 2021) or flows around aerodynamic (Zocca et al., 2019) or bluff bodies (Reinker et al., 2021), where loss impact on the flow field substantially differ from the case of turbine channel flows. The only exception is the work by (Baumgärtner et al., 2019), in which total pressure is measured downstream a micro supersonic annular cascade operated with air, carbon dioxide, and refrigerant R134a. However, the total pressure is measured downstream the probe-induced shock, with the only option of retrieving numerically the total pressure downstream the cascade. Moreover, measurement space resolution is limited by the miniaturization of the cascade and in the design operating conditions the state of the fluid is mildly non-ideal for R134a (minimum compressibility factor $Z = 0.88$) and approximately ideal for the others ($Z \approx 1$). Therefore, the experiments are essentially devoted to evaluate the effect of fluid molecular complexity in wake losses, rather than validate CFD simulations in highly non-ideal conditions typical of ORC turbine operations.

Aiming at assessing CFD calculations employed to verify loss correlations applied to ORC turbine rows, an experimental campaign is under development on an ORC linear cascade, assembled on the Test Rig for Organic VApors (TROVA) of Politecnico di Milano. The test section consists in a supersonic converging-diverging nozzle blade row, designed to operate at nominal outlet mach number of 1.6 (typical of highly loaded stages) with siloxane MM (hexamethyldisiloxane), a working fluid employed in high temperature ORCs. Te fluid thermodynamic conditions envisaged for tests span from highly non-ideal states (inlet total pressure and temperature $P_T \approx 25$ bar, $T_T \approx 260$ °C, corresponding to compressibility factor as low as $Z \approx 0.3$) to dilute gas conditions. For CFD validation purposes, the evaluation of total pressure losses across the row is addressed as the experiment main objective. This in turn requires to measure total conditions P_T, T_T upstream and total pressure downstream the cascade. Schlieren visualization are also considered as a complementary technique to visualize fish tail shock pattern departing from blade trailing edge. The paper reports the full process of experiment design, which substantially differ from the case of conventional blade cascades (typically tested in cold-flow facilities using air at low temperature and pressure) due to challenging operating conditions and the need of complying with space constraints dictated by the test section geometry, while keeping at the same time the high spatial resolution needed for CFD validation. The design of experiment included blade shape definition and optimization in annular configuration, followed by their adaptation in planar cascade within the TROVA test section (including boundary walls) and structural verification. Also, instrument arrangement and traversing system were devised and designed. CFD simulations were largely employed for blade profile optimization in annular row, while the whole flow simulation within the final planar cascade layout is still in progress and can be addressed as the last step preceding the experiments performance.

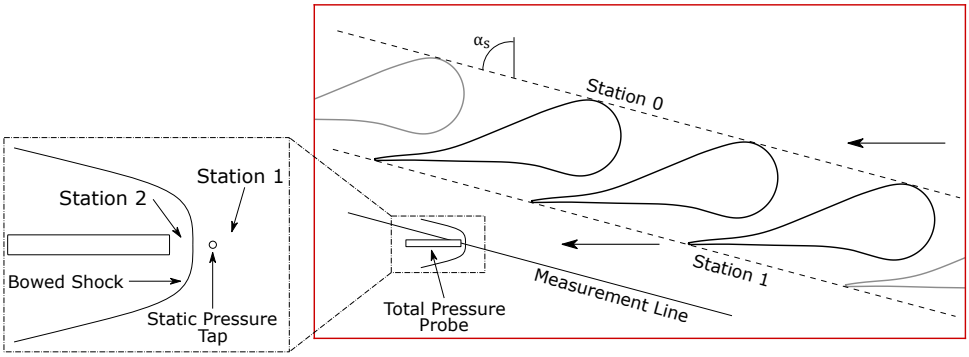

Figure 1: Test section sketch.

2. CONCEPT OF THE CASCADE EXPERIMENT

Aiming at validating CFD-based tools, the experiment arrangement was conceived to meet multiple needs. Designing a cascade geometry representative of actual high-temperature and high-expansion ratio turbines was deemed key, as well as operating the blade row with a fluid and at the thermodynamic conditions relevant for state-of-the-art and innovative high-temperature ORC power plants. Also, simplified solutions were devised for test section layout, instrument equipment, and for the test run procedure. Finally, the application of proven measurement techniques for organic vapors was envisaged.

The typically high value of the turbine stage expansion ratio, coupled with the low speed of sound of organic compounds, generally lead to supersonic flows at the first stator outlet. Therefore, a convening-diverging geometry was chosen as representative of ORC turbine nozzle. An illustrative sketch of the test section is reported in Figure 1, while the design details are discussed in sections 4.2 and 4.3. The cascade, constrained by the limited dimensions of the test section plate (red box in Figure 1), features three complete blades, defining two central channels, together with two partial profiles at the boundaries of the domain, sketched for clarity (in grey). They are replaced by side-walls in the final cascade layout (see Section 4.3), designed to improve flow periodicity and reduce shock disturbances at the measurement points. The blade profile of Figure 1 is to be considered a baseline geometry, derived from an axial ORC stator investigated in (Romei et al., 2020) and adapted to the present experiment to obtain a linear cascade configuration. The baseline shape is optimized to minimize cascade entropy production, as described in Section 4.2. A stagger angle of $\alpha_s = 75°$ (see Figure 1) was selected for the cascade to be consistent with the application considered and to reduce, at the same time, the extent of the semi-bladed channel portion. This allows to avoid a markedly stretched configuration, which would conflict with geometrical constraints of the test section, due to the choice of designing the row with inlet and outlet parallel flows (no flow deflection). This option not only notably simplifies the cascade assembly in the TROVA test section, but also turns out to be representative of radial inflow nozzles, which typically receive rather tangential flow from the volute and are characterized by almost straight camberlines producing small flow deflections. Moreover, as proven in Section 4.2, this configuration is also relevant for axial turbine supersonic stators, which are mostly front-loaded, with flow turning (even remarkable) almost completed through the converging portion, while most of the entropy production occurs in the diverging part of the channel. Additionally, as long as supersonic flows are established, the flow rotation upstream the throat does not affect the downstream flow-field topology.

Total pressure is measured at both cascade inlet P_{T0} and outlet P_{T1}. As illustrated in the following P_{T1}, is retrieved by total pressure P_{T2} measured at the head of a recessed stem pressure probe. As depicted in the detail of Figure 1, a detached bowed shock sets up at total pressure probe head, which is a blunt body immersed into a supersonic flow. Considering a flow-aligned probe, the shock is normal in front of the head tap.The total pressure P_{T2} measured by the probe is therefore the one established downstream the shock (station 2 in Figure 1) which is lower than the value downstream the cascade, P_{T1}, due to probe-induced shock losses. Being reasonable to assume an adiabatic flow within the test section, at least two

additional quantities need to be concurrently measured to unambiguously retrieve P_{T1}, as clarified by systems of equations 1, where, from left to right, the thermodynamic model of the fluid, the integral balance equations through an adiabatic normal shock, and the energy equation across sections 0–1 and 0–2 are specified.

$$\begin{cases} h_{T0} = h\left(T_{T0}, P_{T0}\right) \\ h_1 = h\left(\rho_1, P_1\right) \\ h_2 = h\left(\rho_2, P_2\right) \\ s_2 = s\left(\rho_2, P_2\right) \\ s_2 = s\left(h_{T2}, P_{T2}\right) \end{cases}, \quad \begin{cases} \rho_1 V_1 = \rho_2 V_2 \\ \rho_2 V_2^2 - \rho_1 V_1^2 = P_1 - P_2 \\ h_1 + \frac{V_1^2}{2} = h_2 + \frac{V_2^2}{2} \end{cases}, \quad \begin{cases} h_1 + \frac{V_1^2}{2} = h_{T0} \\ h_{T2} = h_{T0} \end{cases}, \tag{1}$$

where V_1 and V_2 represent, respectively, the velocity components upstream and downstream the normal portion of the bowed shock. Equations 1 form a system of 10 mathematical relation in 12 unknowns, namely h_1, P_1, ρ_1, h_2, P_2, ρ_2, s_2, V_1, V_2, h_{T0}, h_{T2}, and T_{T0}, where h stands for specific enthalpy per unit mass, P for pressure, ρ for density, s for specific entropy per unit mass, and T for temperature. Subscript T refers to total conditions and subscripts 0, 1, and 2 specify respectively section upstream/downstream the blade row and downstream the probe-induced shock. To attain a well-posed mathematical problem, two independent additional quantities are required, namely the inlet total temperature T_{T0} and the static pressure P_1 upstream the probe-induced shock, which need therefore to be measured. Summarizing, total pressure loss assessment through the cascade demands for the concurrent measurements of the inlet total conditions P_{T0}, T_{T0}, of the static pressure downstream the cascade P_1, and of the total pressure at the probe head P_{T2}.

3. DESCRIPTION OF THE EXPERIMENTAL FACILITY

The experimental campaign is designed to be carried out on the Test Rig for Organic VApors (TROVA). The detailed description of the facility and of its operation can be found in (Spinelli et al., 2010, 2013; Pini et al., 2011). The TROVA is a blow-down wind tunnel implementing a batch organic Rankine cycle where a stationary test section replace the expander. No mechanical energy is extracted from the plant, and the whole energy introduced into the system (essentially in thermal form) needs to be rejected to the ambient. The facility is capable of operating at high non-ideal flow conditions with maximum pressure and temperature of 50 bar and 400 °C respectively, which allow to reach highly non-ideal conditions for a large variety of fluids for ORC applications. Main components of the plant are a 1 m^3 volume high pressure vessel (HPV) where the fluid under scrutiny is charged, typically in two-phase conditions, with a mass defined by the desired test operating conditions in terms of pressure and temperature. To attain test conditions starting from ambient temperature and the related saturation pressure, the fluid is isochorically heated via the external electrical tracing of the HPV and of the pipeline upstream the test section, which is also heated in order to avoid fluid condensation during experimental runs. An insulation layer of the heated portion of the plant strongly limits heat dissipation toward the environment. Once test conditions are reached (several hours are required), the opening of a series of valves starts the test, feeding the test section with organic vapor flow at saturated, superheated, or supercritical conditions. Test typically last from tens to hundreds of seconds depending on operating conditions and test section passage area, since both affect the discharged mass flow rate. Despite the transient operation, a quasi-steady flow field establishes in the test section which features a characteristic time order of magnitude lower with respect to the HPV emptying process one; also, flow properties are measured with sufficiently high frequency response instrumentation. The vapor exhausted from the test section is discharged into a 6 m^3 volume low pressure vessel (LPV) where it is de-superheated and condensed through a thermal oil heat exchanger, located at the LPV shell and integrated with a cooling tower circuit and a plate oil/water heat exchanger. Finally, a metering pump closes the loop by pumping the liquid working fluid back to the HPV.

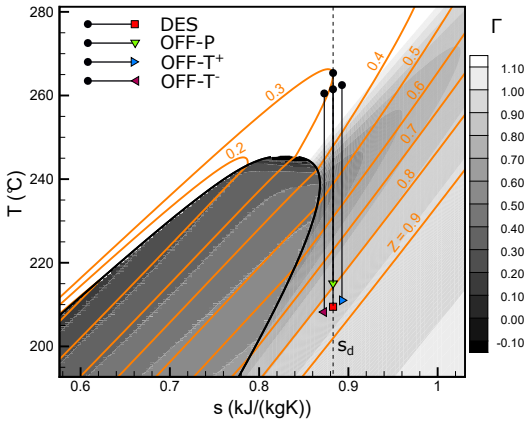

(a) T-s plot of reference isentropic expansions for MM vapor in both design and off-design conditions. The contour of Γ are reported as well as Z isolines.

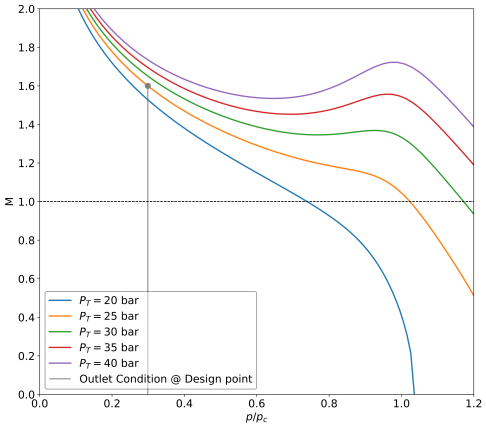

(b) Mach number distribution as a function of reduced pressure P/P_c along isentropic expansions of MM vapor characterized by the same entropy but different stagnation pressure.

Figure 2: Temperature-specific entropy diagram (left) and Mach-reduced pressure representations (right) of MM vapor isentropic expansions. P_c is the fluid critical pressure.

4. DESIGN OF THE EXPERIMENT

4.1 Selection of the operating conditions

All calculations described in the following, including CFD simulations, were performed by applying a state-of-the-art Helmoltz energy equation of state (Span and Wagner, 2003) for MM (Thol et al., 2016), implemented in the NIST RefProp database (Lemmon et al., 2018). Total inlet conditions (station 0 in Figure 1) in both design and off-design conditions were chosen to carry out expansion processes featuring highly non-ideal fluid thermodynamic states, as pointed out in (Romei et al., 2020). The nominal inlet total state (labelled as *DES* in Figure 2a) was computed determining an inlet specific entropy as close as possible to vapour saturation to enhance non-ideal effects along the expansion and to allow the execution of tests in off-design conditions in both temperature and pressure (labels *OFF* in Figure 2a). The design entropy and total pressure were set to s_d = 0.883 kJ/(kgK) and P_{Td} = 25 bar as shown by line *DES* in Figure 2a, which also points out how the expansion crosses a thermodynamic region exhibiting low values of both compressibility factor Z and fundamental derivative of gas dynamics Γ. The latter experiences also significant gradients. This choice of conditions allows to widen the explored range of non-ideality within a single test run, while keeping at the same time sufficient safety margin with respect to both test section maximum pressure and fluid thermal stability limit. Figure 2b shows several isentropic expansions for different values of the inlet total pressure and temperature, the latter being computed from P_T and entropy s_d. The expansions depicted clarify as the design inlet total pressure was selected as an acceptable trade-off between the purpose of attaining remarkable non-ideal gas-dynamic effects and the need to comply with safety constraints. The corresponding inlet total temperature results equal to 261.5 °C. The outlet static pressure, marked with a circle in Figure 2b, was chosen to have a large outlet Mach number, typical of high expansion-ratio applications, without relegating the non-ideal effects in a small region close the nozzle throat. The design outlet Mach number was thus set equal to about 1.6, leading to an outlet static pressure of 5.77 bar, computed through one-dimensional theory. Three possible conditions, reported in Figure 2a, were identified to investigate cascade off-design performance; the first one, referred to as *OFF-P*, is characterized by a higher inlet total pressure P_T = 28 bar and $s = s_d$, while conditions labelled as *OFF-T*$^+$ and *OFF-T*$^-$, consider a higher and lower inlet total temperature (±1 °C) respectively and the design P_{Td}. For for such class of off-design conditions non-ideal effects are expected to trigger significant variability in the flow condition, as shown in (Romei et al., 2020).

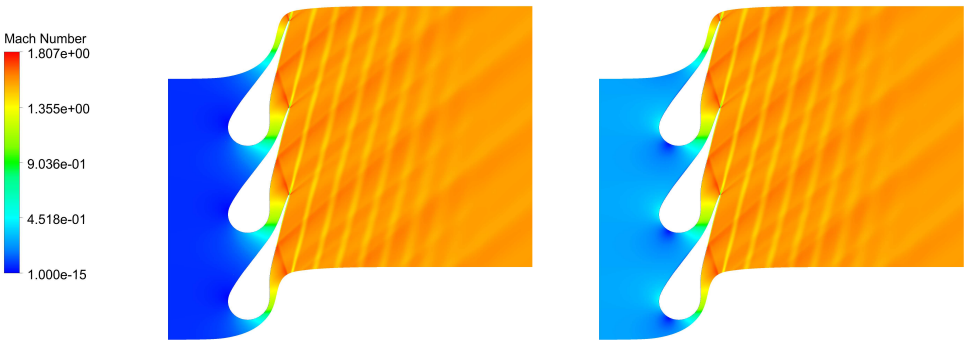

Figure 3: Mach number field. Axial (left) and 75° (right) inlet flow comparison.

4.2 Detailed Blade Design

A further crucial step in the design of such a novel experiment is the identification of a blade shape optimized for operating in the linear cascade, in terms of thermodynamic condition and cascade set-up. To carry out a tailored blade design, computational fluid dynamics (CFD) was systematically applied, at first simulating the baseline profile reported in Figure 1 and then employing a shape-optimization procedure. For these analyses, a periodic annular row is considered, while the effects of the (inevitable) violation of the periodicity among adjacent channels occurring in the actual linear cascade will be considered in studies currently underway. Simulations were performed using the CFD flow model developed at Politecnico di Milano for turbomachinery flow simulations, based on the ANSYS-CFX solver, whose formulation specific for supersonic flows of non-ideal gases is fully detailed in (Persico et al., 2019; Romei et al., 2020). Simulations were performed considering a quasi-3D slice representative of the midspan section of the cascade. The solver integrates the RANS equations, complemented by the turbulence model equations according to the k-ω SST formulation, by resorting to a look-up table approach to introduce the non-ideal thermodynamics of the fluid. The equations were integrated over multi-block meshes composed by about 220000 hexahedral elements, defined after a dedicated mesh-dependence analysis, whose description and result lie outside the scope of the present work, and by assigning $y^+ \leq 1$ at the wall.

Calculations were performed by assigning total pressure, total temperature, flow direction, and turbulence quantities at the inlet, and static pressure at the outlet. The total conditions and the expansion ratio were defined as illustrated in Section 4.1 for the design point (line *DES* in Figure 2a), while the turbulence quantities are assigned following (Romei et al., 2020). A dedicated analysis concerning the inlet flow angle was needed since the cascade configuration is quite different from conventional ones, in which the flow is deflected towards the tangential direction. In this case the blades do not impart any rotation to the flow (as shown in Figure 1). In a conventional configuration, no flow deflection corresponds to operate the cascade with highly negative incidence, therefore preliminary calculations on the baseline are required to investigate the effects of such boundary condition, in particular on the post-throat flow evolution. The baseline geometry was numerically analyzed considering the two limiting conditions of inlet flow angle, measured with respect to the annular row axis, equal to 0° (axial inlet flow) and 75° respectively. Despite the mass flow rate is different in the two cases, due to the assignment of the outlet static pressure as boundary condition, the Mach contour reported in Figure 3 highlights how the two flowfields downstream the sonic throat are almost identical in terms of Mach number value, shock and expansion wave patterns and wake thickness. Obviously, this is not the case of the leading edge region, where the variation of the inlet flow angle leads to different stagnation points, pressure and suction side boundary layers development, and blade pressure distribution. However, thanks to the large radius of curvature at the leading edge, the baseline blade is highly tolerant to the severe change of incidence angle, and no flow detachment is produced. These outcomes are confirmed by the results reported in Figure 4, in which the blade loading (on the right) and the inlet-to-outlet pitchwise mass-averaged pressure distribution (on the left) are compared for the two cases. The pictures highlight how the differences

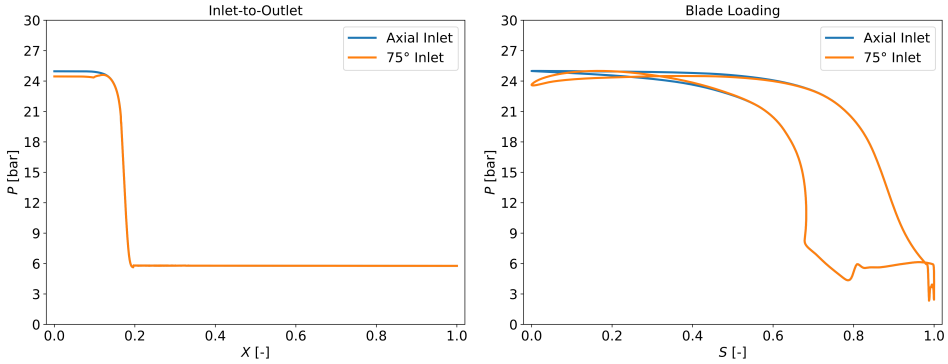

Figure 4: Axial and 75° inlet flow comparison. Inlet-to-outlet pitchwise mass-averaged pressure distribution (left). Pressure distribution along the blade pressure and suction side (right).

in terms of blade loading and pressure distribution occur only in the front part of the blade, upstream of the sonic throat. The present comparison corroborates the re-design of the front-section of the blade, with respect to the one described in (Romei et al., 2020). By virtue of its peculiar leading edge shape, the present blade is suitable to accept the meridional flow typical of axial machines as well as the highly tangential swirling flow entering stators of radial-inflow turbines. As a matter of fact, in radial-inflow turbines the distributor supplies an high tangential flow to the nozzle, whose deflection results small and thus close to the one reproduced in the proposed linear cascade experiment.

Even though the baseline blade configuration was already satisfactory, a shape-optimization process was performed to refine the blade shape in the rear part of the channel, especially from the throat section to the outlet, as most of the entropy production in supersonic cascades occurs in this region. The blade design was performed by applying the in-house shape-optimization tool FORMA (Fluid-dynamic OptimizeR for turboMachinery Aerofoils), which optimizes the shape of blade profiles by resorting to surrogate evolutionary strategies, formulated in constrained, multi-point and multi-objective fashion. FORMA combines a B-spline representation of the blade profiles, the CFD model previously presented, a Kriging formulation as surrogate, and genetic algorithms. Full details on FORMA can be found in (Persico et al., 2019), where also several examples of optimization for ORC nozzles are presented. The baseline blade was, at first, parametrized using 30 control points (CPs), and only six of them, covering most of the blade suction side, were considered movable during the optimization process; the mobility of such CPs being the design space of the optimization problem. Figure 5a reports both fixed (red dots) and movable (green dots) CPs, as well as the investigated design space (light green region). In this way, the optimization was addressed to the rear section of the blade, as required. The four CPs defining the trailing edge are kept fixed to concurrently avoid its rigid translation and deformation. The two CPs on the

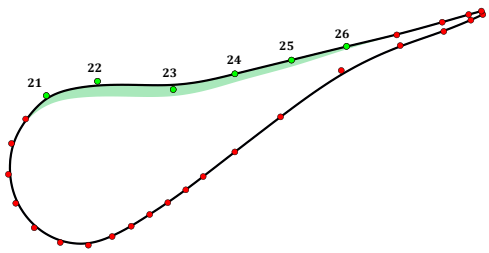

(a) Parametrization of the baseline blade geometry. Red and green dots represent fixed and movable CPs respectively, while the light green region represents the design space.

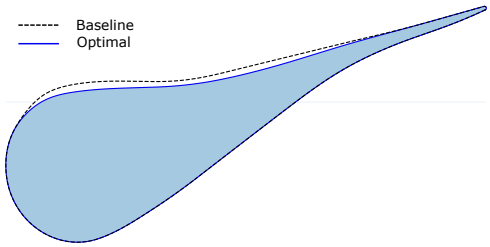

(b) Baseline geometry and optimal blade shape comparison.

Figure 5: Baseline parametrization (left) and optimization procedure results comparison (right).

Table 1: Comparison of baseline geometry with undeformed and deformed optimal blades. Pitchwise mass-averaged flow properties are evaluated at the domain outlet.

	Baseline Blade	**Optimal Blade**	**Deformed Optimal Blade**
Δs [J/(KgK)]	1.757	1.467	1.468
M [-]	1.569	1.574	1.574
α [deg]	75.8	74	73.95
Y_{tot} %	15.27	12.66	12.67

suction side preceding the trailing edge were instead kept fixed to avoid a thinning of the profile, which may lead to non-negligible blade deformations in this region. The global optimization strategy, which was applied for the present optimization problem, involves an initial sampling of the design space for surrogate model interpolation including 60 cascade evaluations, followed by several training iterations that progressively refine the surrogate as the optimization proceeds towards the optimum. Additionally, a constrain was imposed to ensure a flow angle at the domain outlet larger than 74°. The optimization procedure was stopped after 48 iterations of the training phase, leading to 108 total cascade evaluations, since a stable convergence between the surrogate and high-fidelity CFD results was reached. The baseline and optimal blade shapes are compared from a geometrical point of view in Figure 5b, while Figure 6 reports the corresponding Mach fields and Table 1 summarizes the pitchwise mass-averaged values of the main flow properties at the domain outlet for the two configurations. In the table Y_{tot} represents the total pressure loss coefficient, defined as $Y_{tot} = \left(P_{T,up} - P_{T,dn}\right) / \left(P_{T,dn} - P_{dn}\right)$, with subscript *up* and *dn* referring to upstream and downstream blade conditions respectively. Besides the outlet Mach number is slightly larger, the optimal blade is characterized by lower Mach number values within the supersonic diverging portion of the channel. This contributes to prove that in the optimal configuration the flow undergoes a milder pressure drop up to the design outlet one, leading to weaker fishtail shocks and, consequently, to lower entropy production and total pressure losses, as highlighted in Table 1 by the values of Δs and Y_{tot}.

Since the optimal blade (as well as the baseline one) is characterized by a very thin tail, being the thickness lower than 3 mm for a non-negligible portion of the profile up to 0.5 mm at the trailing edge, its structural integrity and the expected deformation due to the blade loading have been assessed by means of finite element method analyses (FEM). FEM simulations were performed using the Abaqus/CAE solver, a module of Abaqus FEA software (Smith, 2009). The pressure distribution retrieved from CFD results was imported in the software and applied as an external load acting on the blade surface, while the geometry was fixed according to the actual dowel-clamping mechanism employed in the experiment. The resulting maximum stress turned out to be much lower than the material yielding limit, while the maxi-

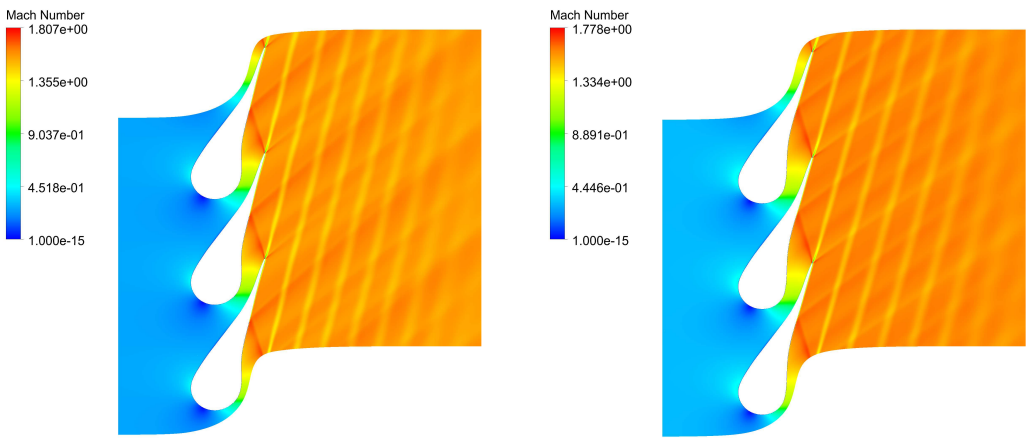

Figure 6: Mach number field. Baseline (left) and optimal (right) blade comparison.

mum deformation was found to be of about 0.1 mm. To investigate the effect of the blade deformation on the resulting flow-field downstream the throat section, the deformed blade geometry was numerically investigated in annular cascade configuration, exploiting the same numerical set-up previously described. The results, in terms of pitchwise mass-averaged flow properties at the domain outlet, are reported in Table 1, in which they are compared to those of the baseline and of the optimal undeformed blade. Clearly, the deformation field caused by the blade pressure distribution does not produce any remarkable variation on the resulting flow-field, being the differences between undeformed/deformed blade configurations lower than the uncertainties related to numerical discretization.

4.3 Test Section Arrangement

The cascade implements three complete blades featuring the optimized profile and arranged horizontally to attain a stagger angle α_s = 75° as illustrated in Figures 1 and 7. The blade row is then completed by partial pressure side (bottom right in Figure 7) and suction side (top left in Figure 7) profiles, integrated into two side-walls bounding the flow field upstream and downstream the cascade. Therefore, the flow delivered by two complete blade channels, including three wakes (one central, two lateral), is expected to be available for characterization downstream, over two full blade pitches along a measurement line parallel to the trailing edge locus. The preliminary design of side-walls was carried out aiming at reproducing the flow streamlines simulated in the annular row configuration (see Figure 7), thus improving cascade periodicity. A refinement was then performed through 3D CFD simulations of the full cascade geometry to attain a higher level of periodicity, and to minimize disturbances at the measuring points due to fishtail shocks departing from trailing edges and their reflections. The cascade is closed on the front and rear side through planar endwalls. On the rear steel plate, blades and sidewalls are dowel-fixed and pressure taps and instrument accesses are machined. The plate is mirror polished and the front endwall is made by a quartz window; this allow to perform schlieren visualization in double-passage configuration. Main dimensions characterizing the cascade are a pitch of 45 mm, a blade chord of 66.5 mm, and a blade height of about 19 mm. The throat width in the blade-to-blade plane is approximately 5.5 mm.

The cascade inlet flow comes from a settling chamber (plenum) upstream the test section, with a moderate and smooth acceleration and it is therefore considered uniform. Also, the action of heating system and of insulation on plenum and test section allows to consider the flow adiabatic. Therefore, total condition T_{T0}, P_{T0} are measured within the settling chamber. Total temperature is provided by two thermocouples (of J and K type) with expanded uncertainty of 1 °C. Due to the negligible kinetic energy in the plenum, the total pressure is measured by a wall flush-mounted absolute piezoresistive transducer for high-temperture applications; the expanded uncertainty is approximately 0.1% of the full scale (FS). Due to the inevitable non-uniformity, the downstream flow characterization requires a measurement traversing; a measuring line parallel to the trailing edge locus was selected downstream, at a distance equal to about the 17% of the blade chord (see Figures 1 and 7). Along this line, the 1.5 mm diameter head of a total pressure probe, pre-aligned with the flow and featuring a recessed stem, is located at different points, which constitute the measuring grid where pressure P_{T2} is measured. The probe head is located at blade mid-span, while at the rear wall, static pressure taps of 0.3 mm diameter are machined at the same positions along the whole measuring grid to retrieve pressure P_1. This is possible thanks to the bow shape of the probe-induced shock and to the two-dimensional nature of the flow. The measuring grid features 21 points along the two central blade pitches (see Figure 7). The grid is not uniformly spaced but refined in the vicinity of the wakes where higher gradients are expected. The total pressure probe access is machined in the steel back plate, as well as the required sealing and rotation/blade-span translation system. Thanks to an already proven test repeatability (Cammi et al., 2021), the probe traversing is obtained with multiple test runs, with one single measuring point accessed at each run. This extends the experimental campaign duration, but entails two indubitable advantages. The first one is to simplify the implementation of the sealing system, since no pitch-wise probe movement is required. The second one is the chance of exploring a wide range of operating conditions in a single test, from highly non-ideal to almost ideal, during the HPV emptying. The measuring system is completed by two rows of 4 static pressure taps arranged at the endwall plate, along the centerline of the diverging portion of the two central channels.

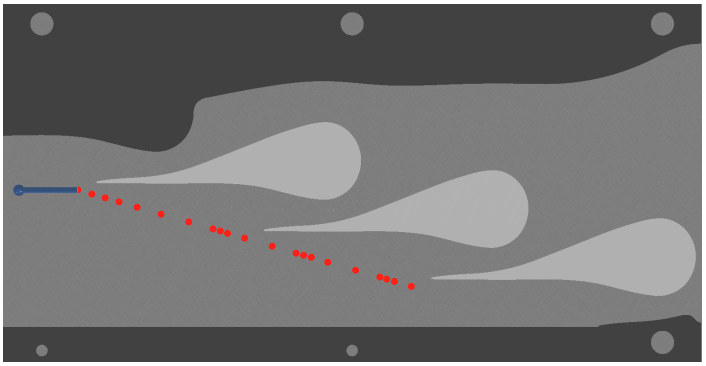

Figure 7: Test section as resulting from preliminary design including side-walls, total pressure probe and downstream measurement points.

Also, a double-passage schlieren equipment is available to visualize the flow field density gradients, highlighting the morphology of shock/fan structures at blade trailing edges and at the probe head with a continuous space resolution. Both, blade passage wall pressure and schlieren images provide significant data to be compared with CFD calculations for validation. All static pressure taps are connected with pneumatic lines, embedded in the heated back plate, to absolute piezoresistive pressure transducer for high temperature, exhibiting 0.1% FS expanded uncertainty. No condensation issues arise, but sensitivity to temperature requires transducers calibration in both pressure and temperature. Contrarily, the total pressure P_{T2} is measured using P_{T0} as reference, via a differential pressure transducer (of 0.05% FS expanded uncertainty) aiming at minimizing uncertainty on loss quantification. Such sensors are for low temperature applications and thus remotely mounted. Therefore, the related pneumatic lines need to be flushed with nitrogen, in order to avoid line condensation and the consequent unacceptable promptness reduction.

5. CONCLUSIONS

The design of an innovative experiment on linear supersonic ORC blade cascade to be carried out on the TROVA facility at Politecnico di Milano is described in this paper. The planned campaign aims at providing relevant experimental data for validation of high-fidelity CFD-based tools currently employed for ORC turbine design, optimization and analysis. The cascade implements a planar converging-diverging nozzle blade row operated with siloxane MM vapor at thermodynamic conditions spanning from highly non-ideal states, in the vicinity of the critical point, to almost ideal gas conditions. The blade profile geometry, derived from an ORC axial stator, was optimized to minimize entropy production and staggered in cascade configuration to accept an inlet flow parallel to the outlet one, namely the flow undergoes no deflection through the finally built blade row. The proposed configuration results to be significant for both axial and radial inflow ORC supersonic stators, these latter experiencing very low flow deflection. The devised measuring system requires the measurement of total pressure and temperature upstream the cascade, as well as the downstream total pressure along a line parallel to the cascade trailing edge. To this purpose, the blade row is traversed downstream with an L-shaped total pressure probe and endwall static pressure taps are machined at same measuring locations, in order to retrieve the total pressure upstream the probe-induced shock, thus allowing to assess losses through the cascade. As complementary measurements, useful for CFD verification, wall static pressure along the divergent portion of two blade passages and schlieren visualization are arranged. Currently, the cascade and measuring system assembly is underway and early tests are foreseen in autumn 2021.

ACKNOWLEDGEMENT

This research is part of the *Energy for Motion* project of the Department of Energy of Politecnico di Milano, funded by the Italian Ministry of University and Research (MUR) through the *Department of Excellence* grant 2018-2022.

REFERENCES

DG Ainley and G Cr Mathieson. A method of performance estimation for axial-flow turbines. Technical report, AERONAUTICAL RESEARCH COUNCIL LONDON (UNITED KINGDOM), 1951.

N. C. Baines, Institution of Mechanical Engineers, and Combustion Engines Group. A meanline prediction method for radial turbine efficiency. Number 11, pages 45–56, Bury St Edmunds, 1998. Professional Engineering Publishing for the Institution of Mechanical Engineers;.

D. Baumgärtner, J.J. Otter, and A.P.S. Wheeler. The effect of isentropic exponent on transonic turbine performance. volume 2C-2019, 2019. doi: 10.1115/GT2019-90251.

F. Beltrame, A.J. Head, C. De Servi, M. Pini, F. Schrijer, and P. Colonna. First experiments and commissioning of the orchid nozzle test section. *ERCOFTAC Series*, 28:169–178, 2021. doi: 10.1007/978-3-030-69306-0_18.

G. Cammi, C.C. Conti, A. Spinelli, and A. Guardone. Experimental characterization of nozzle flow expansions of siloxane mm for orc turbines applications. *Energy*, 218, 2021.

P. Colonna, E. Casati, C. Trapp, T. Mathijssen, J. Larjola, T. Turunen-Saaresti, and A. Uusitalo. Organic Rankine Cycle Power Systems: From the Concept to Current Technology, Applications, and an Outlook to the Future. *Journal of Engineering for Gas Turbines and Power*, 137, October 2015.

H. R. M. Craig and H. J. A. Cox. Performance estimation of axial flow turbines. *Proceedings of the Institution of Mechanical Engineers*, 185(1):407–424, 1970.

Carlo M. De Servi, Matteo Burigana, Matteo Pini, and Piero Colonna. Design method and performance prediction for radial-inflow turbines of high-temperature mini-organic rankine cycle power systems. *Journal of Engineering for Gas Turbines and Power*, 141(9), August 2019. ISSN 0742-4795.

Daniele Fiaschi, Giampaolo Manfrida, and Francesco Maraschiello. Thermo-fluid dynamics preliminary design of turbo-expanders for orc cycles. *Applied Energy*, 97:601–608, 2012. ISSN 0306-2619.

A. J. Glassman. Computer program for design analysis of radial-inflow turbines. Technical report, NASA Technical Note, TN D-8164, Washington D.C., USA, 1976.

A.J. Glassman. Enhanced analysis and users manual for radial-inflow turbine conceptual design code rtd. Technical report, NASA-Contractor Report CR-195454, Washington D.C., USA, 1995.

Angelo La Seta, Andrea Meroni, Jesper Graa Andreasen, Leonardo Pierobon, Giacomo Persico, and Fredrik Haglind. Combined turbine and cycle optimization for organic rankine cycle power systems—part b: Application on a case study. *Energies*, 9(6):393, 2016.

E. W. Lemmon, , Ian H. Bell, M. L. Huber, and M. O. McLinden. NIST Standard Reference Database 23: Reference Fluid Thermodynamic and Transport Properties-REFPROP, Version 10.0, National Institute of Standards and Technology, 2018. URL `https://www.nist.gov/srd/refprop`.

E. Macchi and M. Astolfi. *Organic Rankine Cycle (ORC) Power Systems. Technologies and applications*. Woodhead Publishing Series in Energy: Number 107, Elsevier, New York, 2017.

Andrea Meroni, Miles Robertson, Ricardo Martinez-Botas, and Fredrik Haglind. A methodology for the preliminary design and performance prediction of high-pressure ratio radial-inflow turbines. *Energy*, 164:1062–1078, dec 2018. ISSN 0360-5442.

G. Persico, P. Rodriguez-Fernandez, and A. Romei. High-fidelity shape optimization of non-conventional turbomachinery by surrogate evolutionary strategies. *Journal of Turbomachinery*, 141 (8), 2019.

M. Pini, A. Spinelli, V. Dossena, P. Gaetani, and F. Casella. Dynamic simulation of a test rig for organic vapours. Number PARTS A, B, AND C, pages 1977–1988, 2011. doi: 10.1115/ES2011-54212.

F. Reinker, R. Wagner, L. Hake, and S. der Wiesche. High subsonic flow of an organic vapor past a circular cylinder. *Experiments in Fluids*, 62(3), 2021. doi: 10.1007/s00348-021-03158-y.

M.C. Robertson, P.J. Newton, T. Chen, and R.F. Martinez-Botas. Development and commissioning of a blowdown facility for dense gas vapours. volume 3, 2019. doi: 10.1115/GT2019-91609.

A. Romei, D. Vimercati, G. Persico, and A. Guardone. Non-ideal compressible flows in supersonic turbine cascades. *Journal of Fluid Mechanics*, 882:A121–A1226, 2020. doi: 10.1017/jfm.2019.796.

Michael Smith. *ABAQUS/Standard User's Manual, Version 6.9*. Dassault Systèmes Simulia Corp, United States, 2009.

R. Span and W. Wagner. Equations of state for technical applications. i. simultaneously optimized functional forms for nonpolar and polar fluids. *International Journal of Thermophysics*, 24(1):1–39, January 2003.

A. Spinelli, V. Dossena, P. Gaetani, C. Osnaghi, and D. Colombo. Design of a test rig for organic vapours. In *Proceedings of ASME Turbo Expo, Glasgow, UK*, June 2010.

A. Spinelli, M. Pini, V. Dossena, P. Gaetani, and F. Casella. Design, Simulation, and Construction of a Test Rig for Organic Vapors. *Journal of Engineering for Gas Turbines and Power*, 135, April 2013.

A. Spinelli, G. Cammi, S. Gallarini, M. Zocca, F. Cozzi, P. Gaetani, V. Dossena, and A. Guardone. Experimental evidence of non-ideal compressible effects in expanding flow of a high molecular complexity vapor. *Experiments in fluids*, 59(126), 2018.

Monika Thol, Frithjof H Dubberke, Gabor Rutkai, Thorsten Windmann, Andreas Köster, Roland Span, and Jadran Vrabec. Fundamental equation of state correlation for hexamethyldisiloxane based on experimental and molecular simulation data. *Fluid Phase Equilibria*, 418:133–151, 2016.

M.H. Vavra. Axial flow turbines. *Von Karman Institute for Fluid-dynamics, lecture series 15.*, 1969.

Carlos A. M. Ventura, Peter A. Jacobs, Andrew S. Rowlands, Paul Petrie-Repar, and Emilie Sauret. Preliminary design and performance estimation of radial inflow turbines: An automated approach. *Journal of Fluids Engineering*, 134(3), March 2012. ISSN 0098-2202. doi: 10.1115/1.4006174.

Martin T White and Abdulnaser I Sayma. Simultaneous cycle optimization and fluid selection for orc systems accounting for the effect of the operating conditions on turbine efficiency. *Frontiers in Energy Research*, 7:50, 2019.

M. Zocca, A. Guardone, G. Cammi, F. Cozzi, and A. Spinelli. Experimental observation of oblique shock waves in steady non-ideal flows. *Experiments in fluids*, 60(101), 2019.